Colloid and Polymer Science (2019) 297:989–1000
https://doi.org/10.1007/s00396-019-04527-0

ORIGINAL CONTRIBUTION

Numerical study of wetting stability and sliding behavior of liquid droplets on microgrooved surfaces

Anjan Goswami[1] · Saif Khan Alen[2] · Nazia Farhat[1] · Md. Ashiqur Rahman[1]

Received: 4 December 2018 / Revised: 16 May 2019 / Accepted: 28 May 2019 / Published online: 1 July 2019

Abstract

3D droplet models are developed to numerically investigate the droplet stability and hysteresis of the three-phase contact line on both horizontal and inclined microgrooved solid surfaces. A numerical method is applied to study the shapes and energies of liquid droplets, with a particular focus on the stability of the suspended wetting state. A normalized form of droplet energy is used to compare the relative stabilities of multiple metastable wetting states and a numerical approach is found to reliably predict the wetting stability of droplets on horizontal microgrooved substrates. For wetting on inclined surfaces, numerical simulations of sliding behavior of liquid droplets on flat and periodic microgrooved surfaces with a range of groove geometry are conducted. A numerical model capable of predicting the critical sliding angle of the drop from the knowledge of advancing and receding angles is developed. The effects of microgroove topography, droplet size, and inclination angle on the droplet dynamic behavior are analyzed. Droplet shape and critical sliding angle, obtained from the numerical models, are compared with those of experimental results and are found to be in very good agreement.

Keywords Wettability · Sliding angle · Drop stability · Energetics · Microgrooved surface · Surface Evolver

Introduction

The wetting characteristics of a substrate are dictated by its physical and chemical properties and play a significant role in microfluidic systems [1], pesticide sprays [2], self-cleaning devices [3], refrigeration and air-conditioning systems [4, 5], and so on. The intrinsic wetting behavior of a surface can be manipulated by changing the surface chemistry and/or by introducing roughness into the surface. Introduction of surface roughness can modify the wettability, the way liquid spreads over and wets the surface, and thus can promote the hydrophobicity as well as the water drainage property of the surface [6–13]. Among different ways of roughening a surface, incorporation of microgrooves on the surface is widely used because of its ease in manufacturing and effectiveness in enhancing the wetting behavior.

When a droplet sits on a horizontal microgrooved surface, it can exhibit either Cassie-Baxter (CB) wetting state or Wenzel wetting state depending on the droplet volume and the microgroove geometry [14, 15]. In Wenzel wetting state, droplet enters the asperities of the substrate, whereas in CB wetting state, the droplet remains suspended on the peak of the pillars and contains air pockets. Hence, a composite contact is attained in the CB wetting state and hence this wetting state is termed as "composite wetting." The CB wetting state has received great deal of interest in the recent times because a liquid droplet in composite contact easily moves on the substrate due to reduced resistance [16–26].

On horizontal rough substrates, droplets do not always attain the wetting configuration of absolute minimum energy as predicted by Wenzel and CB models [17, 23]. Depending on how the droplet is formed, droplet may attain the local minimum or a metastable state of the free surface energy. Due to this reason, metastable CB wetting state (advancing or receding), separated by energy barrier from Wenzel state, is observed [17, 22, 27]. Metastable CB droplets on microgrooved surfaces can prevent the wetting transition to Wenzel state,

✉ Md. Ashiqur Rahman
ashiqurrahman@me.buet.ac.bd

[1] Department of Mechanical Engineering, Bangladesh University of Engineering and Technology, Dhaka 1000, Bangladesh

[2] Department of Mechanical Science and Engineering, University of Illinois at Urbana-Champaign, 1206 West Green Street, Urbana, IL 61801, USA

unless significant pressure is applied, the basic requirement for a good superhydrophobic surface [19, 22].

In the recent years, considerable attention has been directed towards the stability of CB wetting state on horizontal microtextured surfaces [16–43]. Through evaporation of droplets, Dubov et al. [28] demonstrated that on a given rough substrate, a minimum size of the droplet is required for stable composite wetting. However, their study was limited to circular pillar–patterned substrates. Zhong et al. [33] emphasized on the density of roughness features for a stable CB state under external pressure. Yang et al. [34] developed a model to determine the critical values of height and pitch of square micropillars to maintain stable CB droplet on with the evolution of droplet evaporation. Using an energy approach, Guo et al. [35] established a generic theory to determine the critical pressure at which CB wetting state collapses on solid surfaces with either porous or protruding microstructures.

However, despite the development of a large number of theoretical models and numerous experimental investigations, numerical methods are still less exploited to explore the factors required for the stability of CB wetting state [38–46]. By computing the minimum energy paths of transition, Pashos et al. [31] developed a numerical method to demonstrate the transition of CB state to Wenzel state on square pillar–patterned surfaces. Chen et al. [32] reported a numerical method to calculate multiple metastable CB on horizontal microgrooved substrate but the study does not include the comparison of stability among different metastable cases. With a specific concentration on the relative stabilities of metastable CB wetting states, Chatain et al. [42] numerically explored the energetics and shape of CB droplets on circular pillar–patterned surfaces. They used a concept of normalized form of droplet energy to compare the stability of metastable droplets. Recently, multiple metastable states of CB droplets deposited on square pillar–patterned surface for a given droplet volume have been systematically simulated [44] by using Surface Evolver (SE) [47]. The relative stability of the CB droplets has been determined by using a dimensionless energy approach. It was found that the solid fraction at the composite drop base plays the key role for the stability of CB wetting state. Semprebon et al. numerically investigated the stability and shape evolution of droplets growing on a large number of V-grooves [45]. Applying the dimensionless energy approach [42], He et al. [46] numerically analyzed the stability of liquid droplets on chemically striped surfaces and reported that a minimum in the dimensionless energy corresponding to the stable wetting configuration is found, as also observed in previous studies [42, 44].

When a surface is tilted through an inclination angle (α), the wetting phenomena becomes different from that typically occurred on a horizontal surface as discussed above. For an inclined substrate, unlike the horizontal surface, the apparent contact angle (angle between the substrate and the droplet) is not uniform along the contact line [48–54]. Instead of forming a uniform apparent contact angle, the droplet makes an advancing contact angle and a receding contact angle with the inclined substrate. Although the intrinsic contact angle is the characteristic property of an ideal surface, real surfaces are characterized by the advancing contact angle and the receding contact angle. Moreover, the gravitational force and surface tension act simultaneously on a sessile drop on inclined substrates.

The research problem of sessile droplets on tilted surfaces has attracted the interest of many researchers [48–62]. Lv et al. [55] have developed an analytical model to determine the sliding angle by using fraction of water-solid interface area, droplet volume, and Young's contact angle. In a recent study, Qi et al. [56] dynamically analyzed the sliding process and sweeping cycle of droplets on sine-shaped microgrooved aluminum surfaces. Very recently, Dai et al. [59] presented the findings of a molecular dynamics simulation on droplet nucleation and transport over liquid infused nano-textures on directional microgrooves. Using Surface Evolver, Xu et al. [60] verified the theoretical morphology features of the molten lead-free solder and analyzed the spreading behavior on an inclined Ni substrate. Santos et al. [53, 54] proposed a numerical model for obtaining the critical sliding angle of a droplet on an incline by analyzing the three-phase contact line force using Surface Evolver. Recently, Qiao et al. [61, 62] investigated the forces involved in the sliding of liquid droplet over microstructured surface.

In the light of the above facts, it is obvious that further numerical studies on the stability of CB state on microgrooved surfaces are required. Moreover, there is a considerable lack of numerical schemes to explore the sliding behavior of droplets on inclined microgrooved substrate. Hence, the present study is structured as follows. Firstly, the stability of the droplet of CB state on microgrooved surfaces is investigated numerically using Surface Evolver. A normalized form of the droplet energy, first introduced by Chatain et al. [42], is used to compare the relative stability of the metastable droplets with different volumes under different wetting configurations. Next, a numerical investigation of sliding behavior of water droplet on inclined microgrooved brass surface is conducted and the results are compared with that of the experimental findings. For this, Surface Evolver is adopted to develop the 3D model of the water droplet on microgrooved brass substrate. The critical sliding angle along the parallel direction to the groove is numerically estimated by analyzing the shape of the contact line and the advancing-receding angles obtained from the simulation.

Model formulation and methodology

The shape of a sessile drop on a substrate is governed by the Young-Laplace equation which balances the surface tension and internal pressure. A variational approach is adopted in this present work for successively minimizing the overall energy of the drop to obtain a final equilibrium shape, and this step was achieved by using Surface Evolver [47]. Surface Evolver works on the principle of minimization of energy and conservation of volume subjected to the constraints and the surface is evolved to a minimum energy via a gradient descent method. In our system, a sessile droplet on a rough solid surface is exposed to air, and its overall energy is the sum of its interfacial potential energy and gravitational potential energy. The interfacial potential energy of the sessile drop can be restricted to the sum of interfacial energies as [44]:

$$E^S = \iint_{A_{LS}} \gamma_{LS} dA + \iint_{A_{LA}} \gamma_{LA} dA + \iint_{A_{SA}} \gamma_{SA} dA \quad (1)$$

where γ_{ij} is the interfacial tension between i and j phases, A_{ij} is the interfacial area between i and j phases, and the subscripts L, A, and S stand for liquid, air, and solid phases, respectively. The local intrinsic contact angle (θ_Y) of the substrate material for each homogenous area can be obtained from the balance of the surface tensions at the three-phase contact line, as defined by Young's equation:

$$\gamma_{SA} - \gamma_{LS} = \gamma_{LA} \cos\theta_Y \quad (2)$$

Using Young's equation, the interfacial potential energy becomes [44]:

$$E^S = \gamma_{LA} \left[A_{LA} - \iint_{A_{LS}} \cos\theta_Y dA \right] \quad (3)$$

The gravitational potential energy of the sessile drop can be expressed as [54]:

$$E^g = -\iiint_V \Delta\rho \vec{g} . \vec{r} dV \quad (4)$$

where $\vec{g}$ is the gravity acceleration vector, r and V are the radius and volume of the droplet, respectively, and $\Delta\rho$ represents the density difference between the liquid and air phases.

Hence, the energy functional of a sessile drop subjected to a fixed volume, expressed by $E = E^S + E^g$, leads to

$$E = \gamma_{LA} \left[A_{LA} - \iint_{A_{LS}} \cos\theta_Y dA \right] - \iiint_V \Delta\rho \vec{g} . \vec{r} dV \quad (5)$$

Liquid droplets on horizontal microgrooved surface

The initial model consists of a three-dimensional drop placed on a horizontal rough substrate patterned with rectangular microgrooves. Study of this section is limited to microdroplets (< 10 μL) for which the gravitational potential energy (E^g) is neglected for the calculation of drop shape. Therefore, for a fixed droplet volume, only the interfacial potential energy (E^S) needs to be minimized to obtain the equilibrium drop shape for a specified intrinsic contact angle.

On a microgrooved surface, a CB droplet forms a composite drop base with alternating solid-liquid and liquid-air contact areas. The liquid-air contact areas are suspended on the microgrooves, and the remaining area of the drop base is formed on the flat solid surfaces in between. Henceforth, for simplicity, the solid portion that forms the solid-liquid contact area between two consecutive microgrooves will be denoted as a "pillar" (Fig. 1). For instance, a droplet having a total of five distinct solid-liquid contact areas at its drop base is denoted as "a droplet on five pillars" and so on.

Simulation of CB droplet on microgrooved surface requires modeling of the wetted top surfaces of the pillars for the solid-liquid interface and free surfaces for the liquid-air interface. Equilibrium drop shapes can be typically obtained by fixing the number of pillars beneath the droplet. In this study, Surface Evolver simulations start with an arbitrary initial shape of the droplet which uses enclosure of triangular facets oriented by the surface normal to represent the body of the model (see Fig. 2a). The vertices belonging to liquid-air interface are not constrained. The free facets of the droplet are given liquid-air interface energy, γ_{LA}, whereas the tension of pillar facets is parameterized by the intrinsic contact angle (θ_Y) as $-\gamma_{LA} \cos\theta_Y$ [38, 43, 46]. The schematic of energy assignment of a droplet in CB wetting state is illustrated in Fig. 1. For all the models, water has been used as the liquid with a liquid-air interfacial tension (γ_{LA}) of 0.072 N/m at 25 °C. On top of the pillar surfaces, the intrinsic contact angle (θ_Y) is fixed at 67.5° (as reported for smooth brass surfaces [9]), and at the location of the grooves, the effective intrinsic contact angle is 180° [38] which leads to $-\gamma_{LA} \cos\theta_Y = -\gamma_{LA} \cos 180 = \gamma_{LA}$ as assigned in our study (Fig. 1).

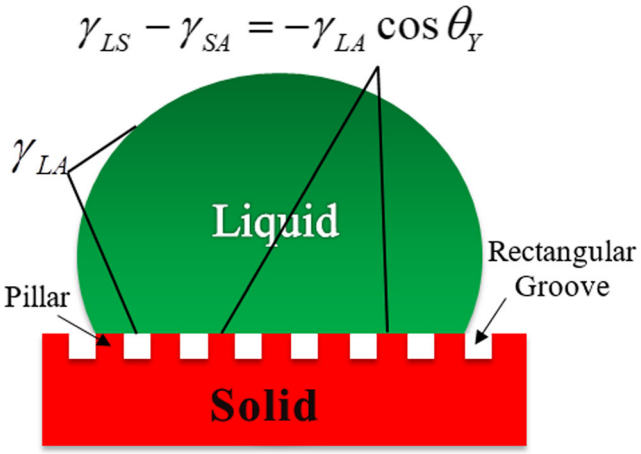

Fig. 1 Schematic of the energy assignment of a CB droplet on microgrooved substrate. The solid portion in between two consecutive microgrooves is denoted as a pillar

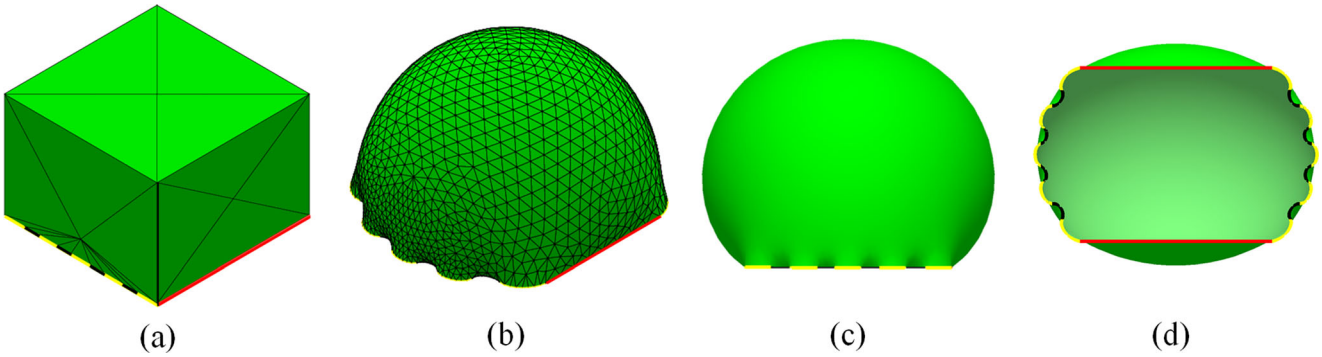

Fig. 2 Simulation of Cassie-Baxter droplet with SE. **a** Isometric view of the initial drop shape on five pillars where constraints are defined. **b** Isometric view of the final drop shape. Pinning of contact line occurs on pillar top surfaces. **c** Rendered front view of the final drop shape. **d** Rendered bottom view of the final drop shape. Straight edges of red color represent the portions of contact line which are constrained to move on the first and fifth pillars. The yellow and black edges represent the portions of the contact line residing on pillar top surface and air, respectively. The alternating yellow-black arcs along with the red edges collectively comprise the composite contact line of the simulated droplet (all the figures are not presented on the same scale)

In the actual model (see Fig. 2), the top surfaces of the pillars, i.e., the facets of solid-liquid interface, are not modeled, rather the energy of the pillar top faces is given to the pillar edges as suggested by Brakke [47]. It is accomplished by converting the area energy integrand to line energy integrand, using an approach similar to that employed in [38, 44, 46, 47]. Assuming $\overrightarrow{S}$ as the oriented droplet surface in contact with the pillar face, T as the contact energy density, and using $\overrightarrow{i}$, $\overrightarrow{j}$, and $\overrightarrow{k}$ as the unit basis vectors, a vector field $\overrightarrow{w}$ can be obtained such that

$$\iint_{\text{face}} T\overrightarrow{k}.d\overrightarrow{S} = \int_{\text{edge}} \overrightarrow{w}.d\overrightarrow{l} \tag{6}$$

where $T = -\gamma_{LA}\cos\theta_Y$. Thus, $\overrightarrow{w} = -Ty\overrightarrow{i}$ or $\overrightarrow{w} = Tx\overrightarrow{j}$ can be used for the line integrals along the three-phase contact line.

Figure 2a shows an initial cubical drop shape when the drop resides on five pillars. The left and right edges of the droplet are constrained to move on the first and fifth rectangular pillars, respectively. The final shape of the numerical simulation, as shown in Fig. 2c, is achieved by successive mesh refinements and energy-minimizing iterative steps along with some intermediate vertex averaging techniques. Repetitions of iteration were continued until the change in the converged free energy was found to be less than 10^{-6} after each successive refinement [38, 43, 46]. The equilibrium droplet shape is found to be anisotropic as displayed in Fig. 2b which is in agreement with the reported studies for droplets on horizontal microgrooved surface [13, 38].

Sliding behavior of droplets on inclined microgrooved surface

Figure 3a shows the schematic of the components of different forces that act on a drop sitting over an inclined surface and Eq. 7 expresses the dimensionless retentive force acting on the drop. The component of the gravitational force tries to move the drop along the inclination of the surface, but hysteresis force, F_h, prevents it from moving until the critical inclination is reached [48, 49]. Critical inclination or sliding angle is defined as the point at which hysteresis force is no longer capable of resisting the drop from moving.

$$\frac{F_h}{\gamma_{LA}L} = k(\cos\theta_{\text{adv}} - \cos\theta_{\text{rec}}) \tag{7}$$

where θ_{adv} and θ_{rec} denote the advancing and receding contact angles, respectively, and k is a constant factor. For describing the behavior of droplet on an incline, the Young-Laplace equation is replaced with the Young-Laplace differential equation, which is more complex.

The simulation is initiated by depositing the droplet on the top of the pillar, and in the case of Wenzel wetting state, the simulation allows the droplet to fill in the grooves, thus not impacting the wetting physics of the simulation. To overcome the singularity of a drop moving from one pillar to its foremost pillar, we have constrained the number of pillars on which the drop can spread. Keeping a fixed droplet volume, the boundary conditions are applied on the contact line of the substrate and on the droplet for simulating the sliding behavior of droplets on inclined substrates. Because of the microscale sizes of the groove, each drop is sitting on multiple grooves, which results in the pinning of the droplet while moving along the grooves. Gravitational force can be included in the model as a function of bond number. Variation of drop shape at different inclination angles is presented in Fig. 3b. In our case, gravity force along the substrate is defined as a function of bond number (Bo) and the inclination angle (α).

$$Bo = \frac{\rho g}{\gamma} V^{2/3} \tag{8}$$

To obtain contact angle hysteresis, the inclination angle of the substrate is initiated as 0° and the equilibrium

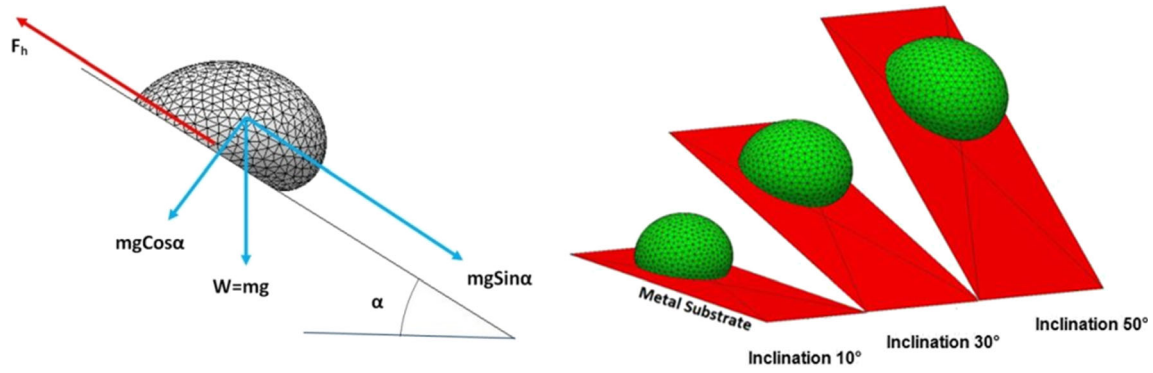

(a) (b)

Fig. 3 **a** Hysteresis force and gravity force acting on a drop on an inclined substrate. **b** Variation of drop shape at different inclination angles (sample $D_G^{67}W_P^{187}W_G^{130}$, drop volume = 35 μL, $\theta_I = 101.2°$, $\theta_{adv} = 119.2°$, $\theta_{rec} = 83.3°$). Here, a sample designation of $D_G^{X}W_P^{Y}W_G^{Z}$ means that the depth of groove is "X," width of pillar is "Y," and width of groove is "Z"

droplet shape is calculated. Once the equilibrium droplet shape is obtained, the required inclination angle of the substrate is introduced keeping the contact line of the drop circular. However, the drop on an inclined microgrooved surface does not have a circular contact line. In order to correct the circular shape of the contact line, experimentally obtained advancing contact angle (θ_{adv}) and receding contact angle (θ_{rec}) are used as constitutive inputs to the model. Unlike pillar width and groove width, Surface Evolver cannot detect the variation of groove depth. However, groove depth is known to play a key role defining the wetting state of the droplet. To overcome this limitation, an analytical model to predict the wetting state of the droplet depending on the topography of the roughness was developed, details of which have been reported elsewhere [7, 63]. Once the wetting state is defined, it is incorporated in the numerical simulation to obtain the equilibrium droplet shape.

To determine the vertex force at each vertex of the base contour, the lengths of the two edges constituting a triple line vertex are calculated. Position of each vertex is corrected by comparing the vertex force, f_i, with the maximum force f_{adv} or f_{rec}. As a result, if the critical inclination angle is reached, the vertices on the contact line will continuously change their position, resulting in a steady moving drop. A similar approach to simulate angular hysteresis is proposed by Santos et al. [53].

$$f_{adv} = \gamma_{LA}(cos\theta_Y - cos\theta_{adv}) \tag{9}$$

$$f_{rec} = \gamma_{LA}(cos\theta_Y - cos\theta_{rec}) \tag{10}$$

Selection of the initial contact angle (θ_I) plays an important role while simulating sliding behavior of a drop on microgrooved surface. In our case, we considered the initial contact angle as defined by Eq. 11, but almost similar result is obtained by using an initial contact angle derived from Eq. 12.

$$\theta_I = \frac{\theta_{adv} + \theta_{rec}}{2} \tag{11}$$

$$\cos\theta_I = \frac{\cos\theta_{adv} + \cos\theta_{rec}}{2} \tag{12}$$

There were several other options of selecting the initial conditions, such as θ_{adv}, θ_{rec}, and $\theta_{intrinsic}$, and simulations were conducted with few of those options in the present study. However, we continued with the assumptions of initial contact angle denoted by Eqs. 11 and 12 as it was found that the simulation converges faster with these assumptions. The critical inclination angle at which the droplet starts to move can be determined from the present model by comparing the numerically obtained advancing and receding contact angles with those of experimental values. The numerical sliding angle is determined by measuring the contact angle hysteresis (CAH) at different inclination angles of the substrate. At first, we obtained the CAH corresponding to the inclination angle of the substrate by using the following approach. When the numerical CAH becomes equal to the experimental CAH, then the corresponding inclination angle is defined as the sliding angle. Using this model, the contact line shape, drop shape, and advancing-receding angle can be obtained accurately by correcting the contact line after every iteration.

Analysis of results

Relative stability of the droplets on horizontal microgrooved surface

In this study, we investigated the multiple metastable CB wetting states of water droplets deposited on horizontal

microgrooved brass surfaces. The stability of the droplets is studied by investigating the changes in shape and energy of the droplets as a function of droplet volume and number of roughness features in contact at the interface. The interfacial potential energy (E^S) that is minimized to get an equilibrium drop shape can be expressed in a normalized form as [44]:

$$E_{\text{norm}} = \frac{E^S}{\gamma_{LA}\left(V^{2/3}\right)} \tag{13}$$

The relative stability of the multiple metastable CB droplets of different volumes can be explored based on a comparison of the dimensionless number, E_{norm}, corresponding to their equilibrium shapes as suggested by Chatain et al. [42]. On smooth flat surfaces, the equilibrium droplets of different volumes possess an invariant E_{norm} value as long as the intrinsic contact angle is fixed for all surfaces. If the surface chemistry, i.e., the intrinsic contact angle changes, E_{norm} value differs. Hence, on a smooth surface, E_{norm} is independent of droplet volume and is solely a function of intrinsic contact angle.

More information regarding this dimensionless number can be found elsewhere [44] where the wetting hysteresis of sessile droplets on square pillar–patterned substrates has been explored. It is established that, for a droplet on rough surface, E_{norm} becomes dependent on droplet volume as constraints are induced in the movement of triple line due to roughness features. In the present anisotropic wetting investigation, the variation of total interfacial energy and its normalized form as a function of droplet volume for droplets deposited on five pillars of sample surface $D_G{}^{67}W_P{}^{187}W_G{}^{130}$ is shown in Fig. 4a. The total interfacial energy increases monotonically with droplet volume whereas the normalized energy attains a minimum near a volume of 1.2 μL. This minimum in the normalized energy (E_{norm}) corresponds to the stable CB droplet on this microgrooved brass surface [42, 44, 46]. The contact angle of this CB droplet and the equilibrium contact angle of a free sessile droplet possessing the same E_{norm} on a plain solid surface are identical [42, 46]. For any other volume, an additional elastic energy will be introduced due to the constrained triple line at the boundaries, and the drop shape is metastable [42]. The metastable droplets possess an advancing or receding front and have contact angles other than the equilibrium contact angles (for details of the theory, see reference [44]). Figure 4b shows the top and front views of three droplets; the middle one corresponds to the stable wetting configuration and the other two droplets correspond to metastable cases. The droplet of 0.41 μL possesses a receding front where the triple line slips on the first and fifth pillars in orthogonal direction, resulting in a point contact with them as shown in Fig. 4b. On the other hand, the droplet of 2 μL possesses an advancing front where the pinning of the triple line occurs on the first and fifth pillar edges due to the constraints applied on those edges. It results in greater spreading of droplet in parallel direction of the grooves and higher anisotropy in the drop shape occurs. Hence, the droplet of stable configuration with minimum normalized energy possesses the least anisotropy in shape compared with that for other metastable droplets.

The analysis is further explored for droplets deposited on different numbers of pillars. The normalized energy curves for different calculated wetting configurations are shown in Fig. 5. Each curve possesses a minimum and has been constructed from calculations of droplets having volumes that correspond to the minimum energy value. As discussed earlier, for droplets with fixed number of pillars underneath, the minimum in normalized energy curve represents the stable droplet residing on that pillar arrangement. In the case of stability, a droplet of fixed volume would reside more stably on the configuration which gives comparatively lower normalized energy. Figure 5 also reveals that for a higher volume of liquid droplet, the normalized energy values for configurations with more pillars are lower than those for configurations

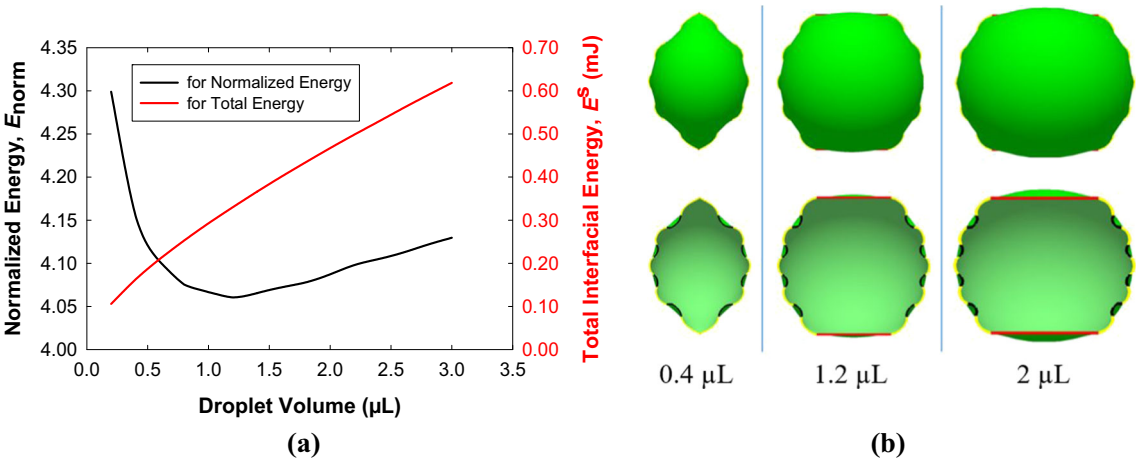

Fig. 4 **a** Variation of total and normalized energy of droplets deposited on five pillars as a function of droplet volume. **b** The top and bottom views of three simulated Cassie-Baxter droplets as a representation of stable and metastable wetting configurations

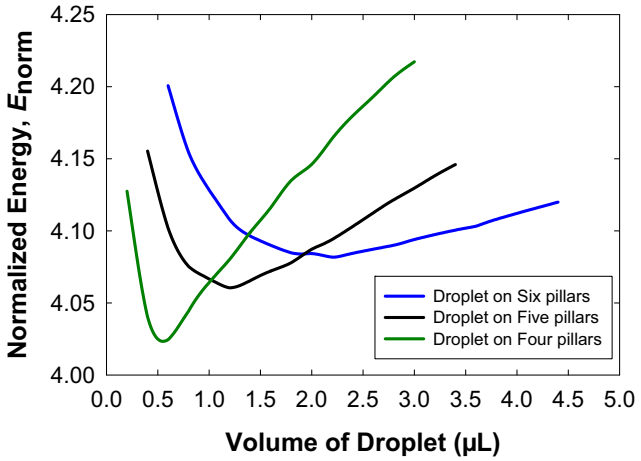

Fig. 5 Variation of normalized energy of droplets of different anisotropic wetting configurations on a microgrooved surface

with fewer pillars. Hence, larger droplet requires more pillars underneath to be stable. As the number of pillars supporting the droplet increases from four to six pillars for the specified brass surface, the size of the stable droplet changes from 0.6 to 2.2 μL. These findings corresponding to the CB wetting on microgrooved surfaces are reminiscent of our previous study of wetting on square pillar–patterned surfaces [44]. Hence, the relative stabilities of CB droplets of different volumes on horizontal microgrooved surfaces can be determined by comparing their normalized energies.

Sliding of liquid droplets on microgrooved surfaces

Sample geometry and experimental sliding angle data

A number of brass surfaces with parallel microgrooves having a wide range of dimensions and fabricated by micromachining were used as sample substrates in an earlier study [9]. Both the depth of groove (D_G) and width of the pillar (W_P) of the microgrooved samples were varied, keeping the width of the groove (W_G) fixed. The results are simulated for droplet volumes of 35 μL, 45 μL, and 60 μL to compare the results on a fixed base for which the experimental data were in hand. The experimental and numerical sliding angles are determined and compared for total eight (08) microgrooved brass samples. For details on the sample geometry, please see elsewhere [9].

The experimental sliding angle measured was the angle of tilt of the substrate when the advancing contact line of the droplet is seen to be in motion even if the receding contact line remains pinned at the same place. The movement of only the leading edge is considered here because from experiment, it was found that the trailing edge of the droplet on few microgrooved surfaces remained attached to the surface even at a high tilting angle. Therefore, in accordance with the experimental observation, in the present study, we defined the critical sliding angle as the angle of tilt at which the forward or advancing edge of the droplet starts to move. The receding contact angle is taken as 0° in cases when the trailing edge of the droplet was found to be pinned on the surface, whereas the advancing edge of the droplet has moved a significant distance.

Comparison and analysis of experimental and numerical results

The numerical model presented here can predict the sliding angle, the contact line shape, and shape of liquid droplets on microgrooved surfaces with the input of experimentally determined advancing and receding angles. The average of these two angles is taken as the initial contact angle (θ_I), which plays a significant role in the accuracy of the numerical results. In our case, a very good agreement between the experimental and the numerical results is found when the initial contact angle is taken to be equal to the average of advancing and receding contact angles. Sliding angle along the parallel direction to the groove is considered in this study. It is because water drainage behavior along the parallel direction to the groove is more meaningful considering the fact that when a drop slides along the orthogonal direction to the groove, pinning occurs at every edge of the groove which resists the droplet motion. Hence, the numerical model developed in this study can be employed in predicting the sliding angle along the parallel direction to the groove.

The variation experimental and numerical critical sliding angles with the width of pillar (W_P) are shown in Fig. 6a. It is found that the results from the numerical model are in a good agreement with those of the experimental findings, and for both cases, the critical sliding angle decreases with the decrease of pillar width. This is because if the pillar width is narrow, then the surface tension acts on a comparatively smaller solid-liquid contact area. Therefore, smaller solid area fraction of the rough surface causes a decrease in the sliding friction and thus facilitates the sliding of a droplet on that surface. Recently, Qiao et al. [61, 62] experimentally demonstrated a similar relationship between sliding friction and solid area fraction for sliding of droplets on both microhole- and micropillar-structured surfaces. In most cases of the present study, the variation between the experimental and numerical values is found to be within ± 2°, but a larger deviation is observed when the pillar width is very small. For this surface (surface with $D_G = 67$ μm and $W_G = 130$ μm), the wetting state was found to be Wenzel, and the experimental receding contact angle was taken as zero (0°) for reasons explained before. In the case of the numerical simulation, for the narrow pillar width (sample $D_G^{67}W_P^{26}W_G^{130}$), the initial contact angle is very small (30.2°). As a result, when the drop obtains an equilibrium shape at zero inclination, the height of the drop is found to be very small. So, when the gravitational force is applied horizontally along the substrate, which indirectly

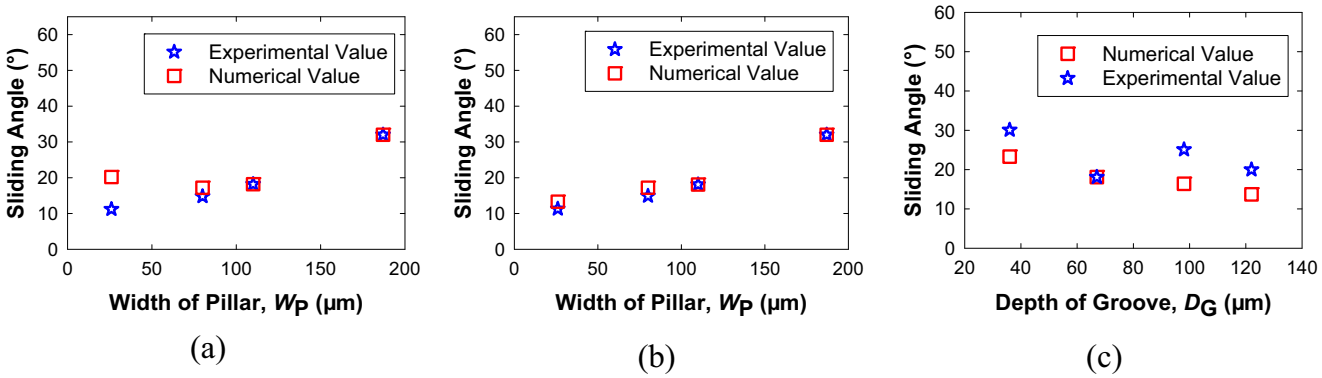

Fig. 6 Comparison between experimental and numerically obtained critical sliding angles for a drop volume of 35 μL and for surfaces with a variation of pillar width and groove depth. These variations are shown for samples with **a** varying pillar width ($D_G = 67$ μm and $W_G = 130$ μm), **b** varying pillar width ($D_G = 67$ μm and $W_G = 130$ μm) and considering receding contact angle 10° for the sample with a pillar width of 26 μm, and **c** varying groove depth ($W_P = 112$ μm and $W_G = 130$ μm)

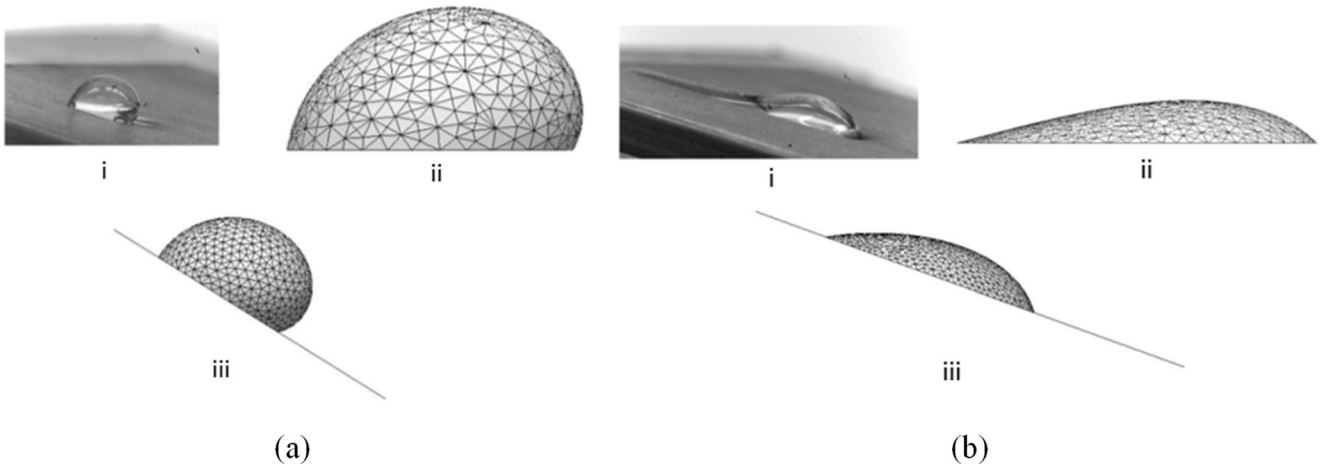

Fig. 7 Comparison of experimental and numerically obtained drop shape at critical sliding angle on microgrooved samples: **a** on sample $D_G^{67}W_P^{187}W_G^{130}$ and **b** on sample $D_G^{67}W_P^{26}W_G^{130}$. Shown in both figures, the experimental drop shape (top left), numerically obtained drop shape where gravity force is implemented as $mg\sin\alpha$ along the substrate (top right), and numerically obtained drop shape where substrate is tilted by critical sliding angle of 32° and 20°, respectively (bottom)

simulates the inclination of the substrate, the gravitational force does not have a considerable impact at the liquid-vapor interface. Therefore, the inclination angle needs to be higher for initiating the sliding motion of the droplet.

However, the difference between the experimental and the numerical values in the case of narrow pillar width is found to be minimized (Fig. 6b) if we consider a small finite value for the receding contact angle of, say 10° instead of 0°, and apply the base contour correction algorithm after every iteration (which is explained earlier in the "Sliding behavior of droplets on inclined microgrooved surface" section). The correction of the base contour was achieved in such a way that the

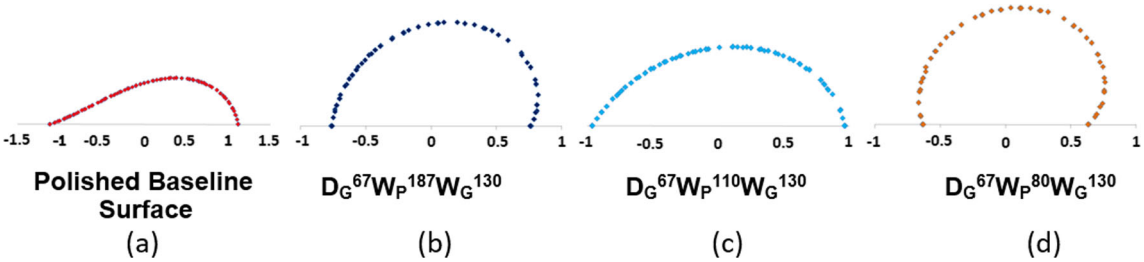

Fig. 8 Drop shape for a drop size of 35 μL at the point of impending motion on **a** polished baseline surface, **b** microgrooved surface $D_G^{67}W_P^{187}W_G^{130}$, **c** microgrooved surface $D_G^{67}W_P^{110}W_G^{130}$, and **d** microgrooved surface $D_G^{67}W_P^{80}W_G^{130}$

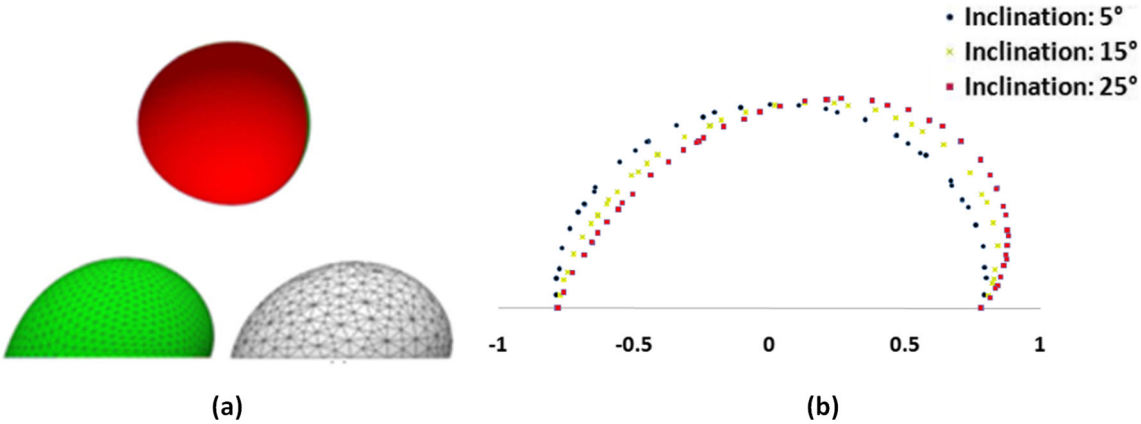

Fig. 9 **a** Drop shape at critical inclination angle by different numerical methods for sample $D_G^{98}W_P^{112}W_G^{130}$. The figure shows the shape of the base contour obtained by using azimuthal angle distribution for apparent contact angle (top), from azimuthal distribution method (bottom left), and the actual shape of the contact line using local contact angle (bottom right). **b** Comparison of drop shape at various inclination angles of the substrate ($D_G^{67}W_P^{187}W_G^{130}$) for a fixed drop size (60 μL)

correction algorithm affects the system's energy functional in a negligible manner. Therefore, the developed numerical model is able to capture the wetting physics and the dynamic wetting behavior of the liquid droplet quite reliably.

The numerical results are found to be in good agreement with the experimental results for samples with a varying pillar width than that with a varying groove depth (Fig. 6c). It can be observed from Fig. 6c that the values of both the experimental and numerically calculated sliding angles decrease with the increase in the depth of the groove. The maximum and minimum deviation of the numerical results from the experimental results is about 10° and 0.15°, respectively.

Comparison and analysis of droplet shape

When a surface is inclined at critical sliding angle, the droplet on it will exhibit an advancing contact angle and a receding contact angle, which can be used to characterize that real surface. So, it is very important to know the shape of the drop as well as the advancing and the receding angles at critical inclination. In this study, the droplet shape with the necessary boundary conditions and inclination of the substrate is obtained from multiple numerical models. These models vary from each other depending on the initialization of the drop and the substrate. Shapes of the droplets from each of these models and from those of experimental findings are almost identical, as shown in Fig. 7a.

If the substrate is kept horizontal, then the inclination is simulated by applying a force, which is a function of bond number and inclination angle, along the length of the surface. But if the substrate with droplet on is inclined, then a constant gravitational energy is simulated for the whole system, which can be seen from Fig. 7a (iii). In the case of a Wenzel droplet, a "tadpole"-shaped droplet is formed with a long tail along the microgrooved surface. This happens due to the pinning of the contact line at the receding edge which does not allow the receding edge to detach even after the advancing edge has moved a significant distance. This phenomenon is also captured successfully in both numerical models; the drop shape comparison for sample $D_G^{67}W_P^{26}W_G^{130}$ (and 45 μL drop volume) from experiment and two numerical models is presented in Fig. 7b.

The numerically determined droplet shapes for microgrooved surfaces and that for a flat surface are compared in Fig. 8. The polished flat baseline surface exhibited a hydrophilic nature and the droplet was found to be elongated in the direction of sliding, as can be seen in Fig. 8a. Whereas the microgrooved brass sample $D_G^{67}W_P^{187}W_G^{130}$ exhibited a large advancing and receding contact angles (117.9°, 81.5°), resulting in a more spherical shape of the drop (Fig. 8b).

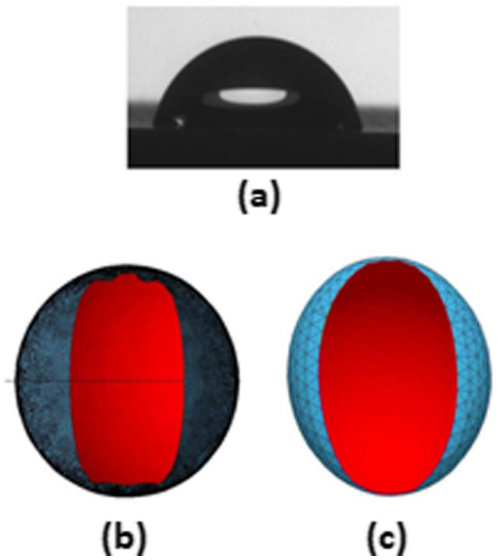

Fig. 10 Drop shape comparison for sample $D_G^{67}W_P^{110}W_G^{130}$ with **a** experimentally obtained sessile drop shape viewed from the parallel direction to the groove, **b** contact line shape from the simulation on rectangular microgrooves, and **c** elliptical contact line due to pinning at the edges

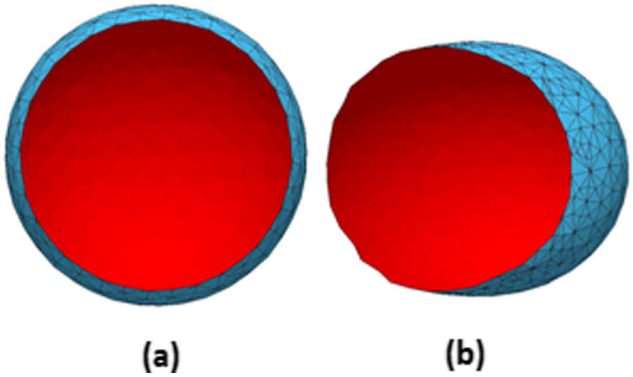

Fig. 11 Correction of base contour (contact line) using vertex force on the triple line for sample $D_G^{67}W_P^{80}W_G^{130}$. **a** Circular contact line. **b** The corrected contact line

Moreover, the spherical shape of the droplet is more pronounced with a decrease of pillar width as observed from Fig. 8c, d. This corroborates our experimental findings as droplets were found to drain more easily from these microgrooved surfaces [9].

To obtain the shape of the droplet at critical inclination angle, ElSherbini and Jacobi [57] suggested an approach of distributing the contact angle on each point of the contact line according to the azimuthal angle of that point. In our study, after obtaining the critical sliding angle from the simulation, the shape of the droplet from the azimuthal distribution is also calculated and a close match between them is obtained, as shown in Fig. 9a. The triple contact line obtained from this approach is almost the same as that has been obtained from our numerical model.

The variation of the shape of the liquid droplet with a change in the inclination angle is displayed in Fig. 9b for the case when the initial contact angle of the drop is more than 90°. Variation of experimental and numerical drop shapes may occur due to the fact of considering equivalent real surface (with advancing and receding angle input) instead of simulating the exact microgroove geometry with boundary conditions. However, the results from experiment and numerical model agree more closely when the shape of the three-phase contact line is corrected by applying the methodology described in the "Model formulation and methodology" section. The present numerical model yields highly accurate results while calculating the sliding angle, and the three-dimensional droplet shapes obtained from the simulation are in very good agreement with experimental findings.

Effects of three-phase contact line on the simulation of sliding behavior

Contact angle hysteresis along the orthogonal direction to the groove is higher than that for the parallel direction to the groove because of the pinning of the three-phase contact line by the pillar edges. If we consider the motion of the drop along the perpendicular direction to the groove, it is observed that the three-phase contact line (base contour) is subjected to energy barrier and gets pinned by the edges of the groove. But no such pinning occurs along the parallel direction to the groove. Sliding of the droplet is always initiated by the movement of advancing end of the contact line. But in the numerical simulations, when critical inclination angle is reached, the drop moves steadily as a whole. On an ideal surface, the three-phase contact line is circular. But heterogeneity of surface deforms the circular shape of the contact line. In the case of microgrooved surfaces, the shape of the three-phase contact line can be elliptical or parallel-sided (Fig. 10a). This is because along the perpendicular direction to the groove, the drop makes a composite surface (in CB state) of solid-liquid and liquid-air contact. The pinning at the edges of the pillars is responsible for this elliptical shape of the contact line which is also corrugated along the perpendicular direction to the groove, as shown in Fig. 10b, c.

Correction of the three-phase contact line shape is necessary after obtaining each equilibrium drop shape. The contact line is corrected to minimize the surface energy and a new

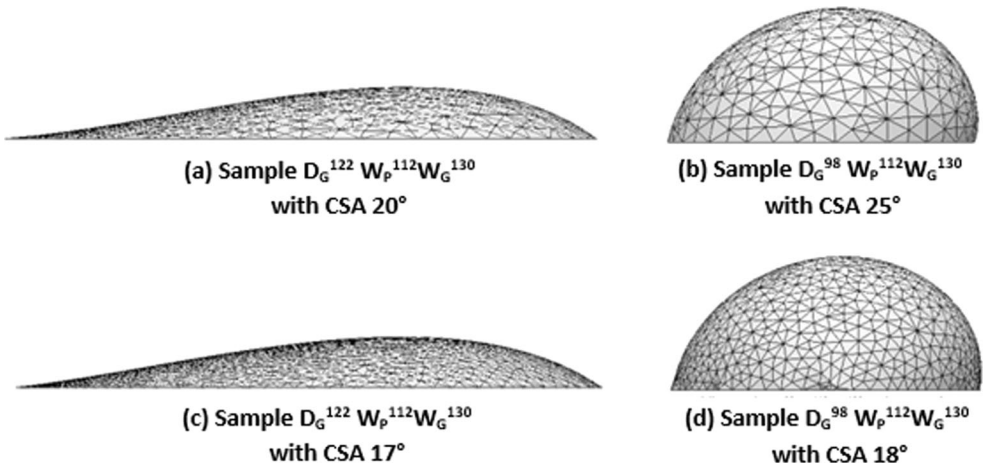

Fig. 12 Comparison of drop shape and critical sliding angle obtained by varying the base contour shape in numerical model. In the top row, critical sliding angle is obtained by keeping the circular shape of base contour **a** for sample $D_G^{122}W_P^{112}W_G^{130}$ and **b** for sample $D_G^{98}W_P^{112}W_G^{130}$. In the bottom row (**c**, **d**), critical sliding angle is obtained by correcting the shape of base contour

equilibrium drop shape is calculated based on the corrected three-phase contact line. For sample $D_G^{67}W_P^{80}W_G^{130}$, with a drop of 35 μL volume, the variation of the circular and the corrected contact line shape is displayed in Fig. 11. The vertex force acting on each vertex constituting the contact line is used to calculate the new positions of the vertices of the contact line, thus forming a new contact line shape. A similar approach of correcting the three-phase contact line is presented by Santos and White [53, 54]. Three-phase contact line correction enhances the numerical accuracy. From Fig. 6c, a significant variation between the experimental and the numerical results was observed. However, if the triple line shape is obtained by numerically calculating the vertex force at each vertex, then the deviation from the experimental results becomes minimal. To illustrate this, from Fig. 12, it is found that for sample $D_G^{98}W_P^{112}W_G^{130}$, the experimentally obtained critical sliding angle is 14.3°, whereas due to the circular base contour assumption, the numerically obtained critical sliding angle is 25°, which has significant deviation from the experimental result. If the base contour of the drop is corrected based on the vertex force at each vertex of the three-phase contact line, then the critical sliding angle reduces to 18°, which reduces the error from ± 10° to ± 4°. Also, in the case of sample $D_G^{122}W_P^{112}W_G^{130}$, a reduction of error by 3° is observed when the three-phase contact line is corrected based on the advancing and receding contact angles of the substrate.

Conclusion

The wetting behavior of liquid droplets on both horizontal and inclined microgrooved surfaces has been studied numerically. For horizontal microgrooved surfaces, due to the slip and pinning of the triple line on the pillars, multiple metastable suspended wetting states (Cassie-Baxter state) were obtained for a given droplet volume. The most stable droplet was found to possess the minimum anisotropy compared with other metastable ones. It has been established that the energetics of wetting and the hysteresis of contact line provide a measure of the stability of the suspended droplets (Cassie-Baxter state) on a horizontal microgrooved substrate. For inclined microgrooved surfaces, a numerical model is developed to characterize the dynamic wetting behavior of the droplet on the substrates. The developed model is capable of predicting the critical sliding angle of the drop by comparing the advancing and receding angles obtained from numerical and experimental findings. The effect of microgroove geometry, droplet volume, and initial conditions on the critical sliding angle is analyzed and compared with the experimental findings. The experimental and the numerical results are found to be in good agreement. The prediction capability of the sliding behavior and shape of the droplet on an inclined surface, as obtained from this study, could be useful in many applications.

Compliance with ethical standards

Conflict of interest The authors declare that they have no conflict of interest.

References

1. Choi CH, Lee H, Weitz DA (2018) Rapid patterning of PDMS microfluidic device wettability using syringe-vacuum-induced segmented flow in non-planar geometry. ACS Appl Mater Interfaces 10(4):3170–3174
2. Zhu L, Ge JR, Qi YY, Chen Q, Hua RM, Luo F, Chen PR (2018) Droplet impingement behavior analysis on the leaf surface of Shu-ChaZao under different pesticide formulations. Comput Electron Agric 144:16–25
3. Liang Y, Ju J, Deng N, Zhou X, Yan J, Kang W, Cheng B (2018) Super-hydrophobic self-cleaning bead-like SiO2@ PTFE nanofiber membranes for waterproof-breathable applications. Appl Surf Sci 442:54–64
4. Lv C, Hao P, Yao Z, Niu F (2015) Departure of condensation droplets on superhydrophobic surfaces. Langmuir 31(8):2414–2420
5. Rahman MA, Jacobi AM (2012). Study of the effects of microgroove geometry on frost structure and properties. International Refrigeration and Air Conditioning Conference at Purdue, West Lafayette, Indiana, USA, 2294
6. Extrand CW (2004) Criteria for ultralyophobic surfaces. Langmuir 20(12):5013–5018
7. Farhat N, Alen SK, Rahman MA (2015) Numerical study of the wetting and mobility of liquid droplets on horizontal and inclined flat and microgrooved surfaces. Procedia Eng 105:576–585
8. Callies M, Quéré D (2005) On water repellency. Soft Matter 1(1):55
9. Rahman MA, Jacobi AM (2012) Wetting behavior and drainage of water droplets on microgrooved brass surfaces. Langmuir 28(37): 13441–13451
10. Patankar NA (2003) On the modeling of hydrophobic contact angles on rough surfaces. Langmuir 19(4):1249–1253
11. Cao L, Hu HH, Gao D (2007) Design and fabrication of microtextures for inducing a superhydrophobic behavior on hydrophilic materials. Langmuir 23(8):4310–4314
12. Extrand CW (2002) Model for contact angles and hysteresis on rough and ultraphobic surfaces. Langmuir 18(21):7991–7999
13. Rahman MA, Jacobi AM (2012) Drainage of frost melt water from vertical brass surfaces with parallel microgrooves. Int J Heat Mass Transf 55(5–6):1596–1605
14. Cassie ABD, Baxter S (1944) Wettability of porous surfaces. Trans Faraday Soc 40:546–551
15. Wenzel RN (1936) Resistance of solid surfaces to wetting by water. Ind Eng Chem 28(8):988–994
16. Rahman MA, Goswami A (2017) Analysis of the energetics and stability of liquid droplets on textures surfaces with square micropillars. 13th International Conference on Heat Transfer, Fluid Mechanics and Thermodynamics, Portoroz, Slovenia
17. Reyssat M, Yeomans JM, Quéré D (2007) Impalement of fakir drops. EPL 81(2):26006
18. Kusumaatmaja H, Blow ML, Dupuis A, Yeomans JM (2008) The collapse transition on superhydrophobic surfaces. EPL 81(3):36003
19. Bormashenko E (2015) Progress in understanding wetting transitions on rough surfaces. Adv Colloid Interf Sci 222:92–103
20. Checco A, Ocko BM, Rahman A, Black CT, Tasinkevych M, Giacomello A, Dietrich S (2014) Collapse and reversibility of the superhydrophobic state on nanotextured surfaces. Phys Rev Lett 112(21):216101

21. Nosonovsky M, Bhushan B (2007) Biomimetic superhydrophobic surfaces: multiscale approach. Nano Lett 7(9):2633–2637
22. Afferrante L, Carbone G (2010) Microstructured superhydrorepellent surfaces: effect of drop pressure on fakir-state stability and apparent contact angles. J Phys Condens Matter 22(32):325107
23. Barbieri L, Wagner E, Hoffmann P (2007) Water wetting transition parameters of perfluorinated substrates with periodically distributed flat-top microscale obstacles. Langmuir 23(4):1723–1734
24. Zheng QS, Yu Y, Zhao ZH (2005) Effects of hydraulic pressure on the stability and transition of wetting modes of superhydrophobic surfaces. Langmuir 21(26):12207–12212
25. Cai TM, Jia ZH, Yang HN, Wang G (2016) Investigation of Cassie-Wenzel wetting transitions on microstructured surfaces. Colloid Polym Sci 294(5):833–840
26. Fang W, Guo H, Li B, Li Q, Feng X (2018) Revisiting the critical condition for the Cassie–Wenzel transition on micropillar-structured surfaces. Langmuir 34(13):3838–3844
27. Bhushan B, Jung YC (2011) Natural and biomimetic artificial surfaces for superhydrophobicity, self-cleaning, low adhesion, and drag reduction. Prog Mater Sci 56(1):1–108
28. Dubov AL, Perez-Toralla K, Letailleur A, Barthel E, Teisseire J (2013) Superhydrophobic silica surfaces: fabrication and stability. J Micromech Microeng 23(12):125013
29. He B, Patankar NA, Lee J (2003) Multiple equilibrium droplet shapes and design criterion for rough hydrophobic surfaces. Langmuir 19(12):4999–5003
30. Dubov AL, Mourran A, Möller M, Vinogradova OI (2015) Regimes of wetting transitions on superhydrophobic textures conditioned by energy of receding contact lines. Appl Phys Lett 106(24):241601
31. Bottiglione F, Di Mundo R, Soria L, Carbone G (2015) Wenzel to Cassie transition in superhydrophobic randomly rough surfaces. Nanosci Nanotechnol Lett 7(1):74–78
32. Zhang X, Zhu W, He G, Zhang P, Zhang Z, Parkin IP (2016) Flexible and mechanically robust superhydrophobic silicone surfaces with stable Cassie–Baxter state. J Mater Chem A 4(37): 14180–14186
33. Long J, Pan L, Fan P, Gong D, Jiang D, Zhang H et al (2016) Cassie-state stability of metallic superhydrophobic surfaces with various micro/nanostructures produced by a femtosecond laser. Langmuir 32(4):1065–1072
34. Wang G, Jia ZH, Yang HN (2016) Stability of a water droplet on micropillared hydrophobic surfaces. Colloid Polym Sci 294(5): 851–858
35. Guo HY, Li B, Feng XQ (2016) Stability of Cassie-Baxter wetting states on microstructured surfaces. Phys Rev E 94(4):042801
36. Zu YQ, Yan YY (2016) Single droplet on micro square-post patterned surfaces-theoretical model and numerical simulation. Sci Rep 6:19281
37. Pashos G, Kokkoris G, Papathanasiou AG, Boudouvis AG (2016) Wetting transitions on patterned surfaces with diffuse interaction potentials embedded in a Young-Laplace formulation. J Chem Phys 144(3):034105
38. Chen Y, He B, Lee J, Patankar NA (2005) Anisotropy in the wetting of rough surfaces. J Colloid Interface Sci 281(2):458–464
39. Gong W, Zu Y, Chen S, Yan Y (2017) Wetting transition energy curves for a droplet on a square-post patterned surface. Sci Bull 62(2):136–142
40. Hao JH, Wang ZJ (2016) Modeling Cassie-Baxter state on superhydrophobic surfaces. J Dispers Sci Technol 37(8):1208–1213
41. Zhang W, Zhang RR, Jiang CG, Wu CW (2017) Effect of pillar height on the wettability of micro-textured surface: volume-of-fluid simulations. Int J Adhes Adhes 74:64–69
42. Chatain D, Lewis D, Baland JP, Carter WC (2006) Numerical analysis of the shapes and energies of droplets on micropatterned substrates. Langmuir 22(9):4237–4243
43. Promraksa A, Chuang YC, Chen LJ (2014) Study on the wetting transition of a liquid droplet sitting on a square-array cosine wave-like patterned surface. J Colloid Interface Sci 418:8–19
44. Goswami A, Rahman MA (2017) Numerical study of energetics and wetting stability of liquid droplets on microtextured surfaces. Colloid Polym Sci 295(10):1787–1796
45. Semprebon C, Herrmann C, Liu B-Y, Seemann R, Brinkmann M (2018) Shape evolution of droplets growing on linear micro-grooves. Langmuir 34(36):10498–10511
46. He L, Sui X, Liang W, Wang Z, Akbarzadeh A (2018) Numerical analysis of anisotropic wetting of chemically striped surfaces. RSC Adv 8(55):31735–31744
47. Brakke KA (1992) The surface evolver. Exp Math 1(2):141–165
48. Janardan N, Panchagnula MV (2014) Effect of the initial conditions on the onset of motion in sessile drops on tilted plates. Colloids Surf A Physicochem Eng Asp 456:238–245
49. Semprebon C, Brinkmann M (2014) On the onset of motion of sliding drops. Soft Matter 10(18):3325–3334
50. Extrand CW, Kumagai Y (1995) Liquid drops on an inclined plane: the relation between contact angles, drop shape, and retentive force. J Colloid Interface Sci 170(2):515–521
51. Gao N, Geyer F, Pilat DW, Wooh S, Vollmer D, Butt H-J, Berger R (2018) How drops start sliding over solid surfaces. Nat Phys 14: 191–196
52. Antonini C, Carmona FJ, Pierce E, Marengo M, Amirfazli A (2009) General methodology for evaluating the adhesion force of drops and bubbles on solid surfaces. Langmuir 25:6143–6154
53. Santos MJ, White JA (2011) Theory and simulation of angular hysteresis on planar surfaces. Langmuir 27(24):14868–14875
54. Santos MJ, Velasco S, White JA (2012) Simulation analysis of contact angles and retention forces of liquid drops on inclined surfaces. Langmuir 28(32):11819–11826
55. Lv C, Yang C, Hao P, He F, Zheng Q (2010) Sliding of water droplets on microstructured hydrophobic surfaces. Langmuir 26(11):8704–8708
56. Qi B, Zhou J, Wei J, Li X (2018) Study on the wettability and condensation heat transfer of sine-shaped micro-grooved surfaces. Exp Thermal Fluid Sci 90:28–36
57. ElSherbini AI, Jacobi AM (2004) Liquid drops on vertical and inclined surfaces: I. An experimental study of drop geometry. J Colloid Interface Sci 273(2):556–565
58. Bhutani G, Muralidhar K, Khandekar S (2013) Determination of apparent contact angle and shape of a static pendant drop on a physically textured inclined surface. Interfacial Phenom Heat Transf 1(1):29–49
59. Dai X, Sun N, Nielsen SO, Stogin BB, Wang J, Yang S, Wong TS (2018) Hydrophilic directional slippery rough surfaces for water harvesting. Sci Adv 4(3):eaaq0919
60. Xu B, Yuan Z, Wu Y (2014) Simulation analysis on surface morphology and hysteresis characteristics of molten Sn–3.0 Ag–0.5 Cu sitting on the inclined Ni substrate. Colloids Surf A Physicochem Eng Asp 441:217–225
61. Qiao S, Li Q, Feng X (2018) Sliding friction and contact angle hysteresis of droplets on microhole-structured surfaces. Eur Phys J E 41(2):25
62. Qiao S, Li S, Li Q, Li B, Liu K, Feng X (2017) Friction of droplets sliding on microstructured superhydrophobic surfaces. Langmuir 33(47):13480–13489
63. Alen SK, Farhat N, Rahman MA (2016) Analytical modeling of wetting states and simulation of drop shape on microstructured surfaces. AIP Conf Proc 1754:050043